Two-Dimensional Room-Temperature Ferromagnetic Semiconductors with Quantum Anomalous Hall Effect

Jing-Yang You⬤,[1] Zhen Zhang,[1] Bo Gu,[2,3,*] and Gang Su[1,2,3,†]

[1]*School of Physical Sciences, University of Chinese Academy of Sciences, 100049 Beijng, China*
[2]*Kavli Institute for Theoretical Sciences, and CAS Center for Excellence in Topological Quantum Computation, University of Chinese Academy of Sciences, 100190 Beijing, China*
[3]*Physical Science Laboratory, Huairou National Comprehensive Science Center, 101400 Beijing, China*

To obtain room-temperature ferromagnetic semiconductors and to realize the room-temperature quantum anomalous Hall effect (QAHE) have been big challenges for a long time. Here we report that, on the basis of first-principles calculations, $PdBr_3$, $PtBr_3$, PdI_3, and PtI_3 monolayers are ferromagnetic semiconductors that could exhibit a high-temperature QAHE. The Curie temperatures estimated by Monte Carlo simulations are 350 and 375 K for $PdBr_3$ and $PtBr_3$ monolayers, respectively. The band gaps of $PdBr_3$ and $PtBr_3$ are found to be 58.7 and 28.1 meV, respectively, with the generalized-gradient approximation and 100.8 and 45 meV, respectively, with the HSE06 method, being quite well in favor of observing the room-temperature QAHE. It is shown that the large band gaps are induced from multiorbital electron correlations. By carefully studying the stabilities of the four aforementioned monolayers, we unveil that they could be feasible for use in experiments. The present work sheds light on the development of spintronic devices by use of room-temperature ferromagnetic semiconductors and the implementation of dissipationless devices by application of the room-temperature QAHE.

I. INTRODUCTION

The realization of materials that combine semiconducting behavior and magnetism has long been a dream of material physics. Magnetic semiconductors have been demonstrated to work at low temperatures but not yet at high temperatures for spintronic applications. "Is it possible to create magnetic semiconductors that work at room temperature?" was selected as one of 125 big questions in *Science* [1]. The highest Curie temperature of the most-extensively-studied magnetic semiconductor (Ga,Mn)As is still far below room temperature [2]. The recent development of magnetism in two-dimensional (2D) van der Waals materials has provided a new class of magnetic semiconductors with possible high Curie temperatures [3].

In 2D systems, magnetism with nontrivial topology can induce unusual behaviors. One example is the quantum anomalous Hall effect (QAHE), which is a quantized Hall effect without an external magnetic field, where the combination of strong spin-orbit coupling (SOC) and ferromagnetic (FM) ordering can generate a band gap in the

bulk and gapless chiral edge states at boundaries, and the quantized Hall conductivity is carried by the edge states [4–9]. Owing to the dissipationless chiral edge states, the QAHE would have potential applications in low-power-consumption spintronic devices [10]. Thus, the search for materials with a QAHE has attracted extensive interest [6,11–15]. Inspired by the seminal work of Haldane [4], the honeycomb lattice is often thought to be a suitable platform for the QAHE. Graphene with enhanced SOC, which can be a topological insulator [16–18], may reveal the QAHE if it is doped with magnetic impurities or through the proximity effect [19–23].

Nonetheless, the QAHE in current experiments is realized only at very low temperature. The first experimental observation of the QAHE was realized in Cr-doped $(Bi, Sb)_2Te_3$ thin film at 30 mK [13]. Later, the QAHE was observed in V-doped $(Bi, Sb)_2Te_3$ thin film at 25 mK [24] and a Cr-and-V-codoped $(Bi, Sb)_2Te_3$ system at about 300 mK [25]. So far, the highest temperature to realize the QAHE is about 2 K in Cr-doped $(Bi, Sb)_2Te_3$ films [26]. In those doped topological insulators, magnetic disorder was found to affect dramatically the temperature at which the QAHE is observed. The edge states are robust against lattice disorder but are greatly affected by magnetic disorder. To obtain a full quantization of the QAHE

in magnetically doped topological insulators, a very low temperature was usually used to suppress magnetic disorders in experiments [7].

To overcome the influence of magnetic disorder, a 2D intrinsic ferromagnetic semiconductor with a finite Chern number is a promising way to realize the QAHE. The QAHE with in-plane magnetization was discussed in Ref. [27], and the QAHE at a temperature of about 20 K was recently proposed in monolayer LaCl with in-plane magnetization [28]. For realistic applications of the QAHE, new materials with a room-temperature QAHE are highly desired. Several ferromagnetic transition-metal trihalides were proposed to be candidates for the realization of the QAHE [29–33]. Among them a $PdCl_3$ monolayer was predicted to be a promising candidate for realizing the QAHE at high temperature.

To find QAHE materials more feasible for use in experiments, we notice that bulk $PtBr_3$ was synthesized and described by Wöhler and Müller [34] in 1925 and single crystals of dark-red $PtBr_3$ were grown in 1969 [35]. Here we show that, by first-principles calculations, $PdBr_3$ and $PtBr_3$ monolayers with a honeycomb lattice are 2D ferromagnetic semiconductors with out-of-plane magnetization that can also realize the QAHE at quite high temperature, where the Curie temperature T_C and band gap E_g/k_B are shown to be higher than room temperature. The large band gap, opened by the spin-orbit coupling, comes from the multiorbital electron correlations. By our calculations, $PtBr_3$ and $PdBr_3$ monolayers are shown to have free energies and formation energies both lower than the recently proposed $PdCl_3$ monolayer [33], indicating that 2D $PdBr_3$ and $PtBr_3$ may be promising candidates for realizing the room-temperature QAHE in experiments.

The first-principles calculations are performed with VIENNA AB INITIO SIMULATION PACKAGE with use of the projector-augmented-wave method in the framework of density-functional theory [36,37]. The electron exchange-correlation functional is described by the generalized-gradient approximation (GGA) in the form proposed by Perdew *et al.*, [38]. The structure relaxation considering both the atomic positions and the lattice vectors is performed by the conjugate-gradient scheme until the maximum force on each atom is less than 0.0001 eV/Å, and the total energy is converged to 10^{-8} eV with a Gaussian-smearing method. To avoid unnecessary interactions between the monolayer and its periodic images, the vacuum layer is set to 15 Å. The energy cutoff of the plane waves is chosen as 550 eV. The Brillouin-zone integration is sampled by use of a $13 \times 13 \times 1$ G-centered Monkhorst-Pack grid for the calculations of relaxation and electronic structures. The phonon frequencies are calculated by a finite-displacement approach as implemented in PHONOPY [39], in which a $3 \times 3 \times 1$ supercell and a displacement of 0.01 Å from the equilibrium atomic positions are used. SOC is included by a second variational

procedure on a fully self-consistent basis. An effective tight-binding Hamiltonian constructed from the maximally localized Wannier functions is used to investigate the surface states [40,41]. The iterative Green function method [42,42] is used with the package WannierTools [43].

II. RESULTS

The structure of the $PdBr_3$ ($PtBr_3$) monolayer, the space group of which is $P\bar{3}1m$ (no. 162), is depicted in Fig. 1(a). Each primitive cell contains two formula units of $PdBr_3$ ($PtBr_3$) and has two Pd (Pt) atoms. Under the crystal field of the surrounding Br octahedra, the d orbitals of the two Pd (Pt) atoms split into threefold t_{2g} orbitals and twofold e_g orbitals, where the latter are energetically higher. For Pd^{3+} (Pt^{3+}) with seven electrons in the $PdBr_3$ ($PtBr_3$) monolayer, since the crystal field is strong, six electrons will fill the t_{2g} orbitals and the remaining one will fill the e_g orbitals, leading to the spin $S = 1/2$. To confirm the stability of the $PdBr_3$ ($PtBr_3$) monolayer, its phonon spectrum is calculated. There is no imaginary-frequency mode in the whole Brillouin zone, as shown in Figs. 1(b) and 1(c), indicating that the $PdBr_3$ and $PtBr_3$ monolayers are dynamically stable.

The structural stabilities of $PdBr_3$ and $PtBr_3$ are also examined by the formation energy (Table I) and the free energy (Fig. 2). The negative values obtained, $E_f = -0.08$ eV for the $PdBr_3$ monolayer and $E_f = -2.41$ eV for the $PtBr_3$ monolayer, are indicative of an exothermic reaction. We also calculate a formation energy of 0.01 eV for the $PdCl_3$ monolayer using the same method as for $PdBr_3$
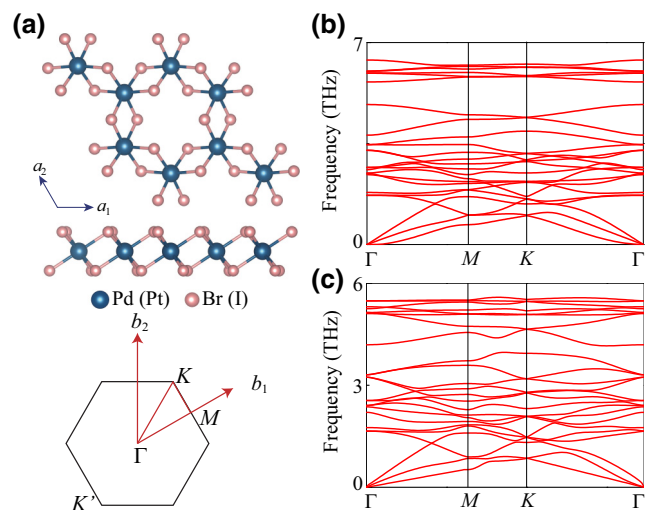

FIG. 1. Stable structures of 2D $PdBr_3$ and $PtBr_3$ monolayers with a honeycomb lattice. (a) Top and side views of the $PdBr_3$ ($PtBr_3$) monolayer as well as the first Brillouin zone with high-symmetry points labeled. Pd (Pt) atoms form a honeycomb lattice, and a unit cell contains four Pd (Pt) atoms. Phonon spectra of (b) $PdBr_3$ and (c) $PtBr_3$ monolayers.

TABLE I. Formation energy E_f for PdBr$_3$, PtBr$_3$, PdI$_3$, and PtI$_3$ monolayers, as well as the PdCl$_3$ monolayer for comparison, calculated by $E_f = E(AB_3) - E(A) - (3/2)E(B_2)$, where $E(AB_3)$ and $E(A)$ are the total energies of the PdBr$_3$ (PtBr$_3$, PdI$_3$, and PtI$_3$) and Pd (Pt) crystals, respectively, and $E(B_2)$ is the total energy of the Br$_2$ (I$_2$) molecule.

	PdBr$_3$	PtBr$_3$	PdI$_3$	PtI$_3$	PdCl$_3$
E_f (eV)	-0.08	-2.41	0.13	-2.44	0.01

and PtBr$_3$, which can thus be compared reasonably at the same level. The lower formation energy and lower free energy for the PdBr$_3$ and PtBr$_3$ monolayers compared with the PdCl$_3$ monolayer indicate that they are more feasible for use in experiments.

To determine the ground state of the PdBr$_3$ monolayer, in the absence of SOC, we calculate the total energy for FM and antiferromagnetic (AFM) configurations as a function of the lattice constant, and find that the FM state has energy lower than the AFM state. The equilibrium lattice constant of PdBr$_3$ for the FM state is $a_0 = 6.667$ Å in Fig. 3(a). The PtBr$_3$ monolayer also has a ferromagnetic ground state, but with a larger lattice constant, $a_0 = 6.732$ Å.

The electronic band structure without inclusion of SOC [Fig. 3(b)] shows that the PdBr$_3$ monolayer is a Weyl half-metal, which acts as a conductor with only one species of electron-spin orientations at the Fermi level and at the high-symmetry K point there is a Weyl node protected by the C_{3v} space group. Because of the inversion symmetry, there is another Weyl point at K'. The total density of states is contributed mainly by p electrons of Br atoms and e_g electrons of Pd atoms.

In the presence of SOC, the magnetic anisotropy should be considered. To determine the magnetic behavior of PdBr$_3$ and PtBr$_3$ monolayers, we calculate the total energy of PdBr$_3$ and PtBr$_3$ monolayers with different possible configurations of Pd and Pt spins on the honeycomb lattice,
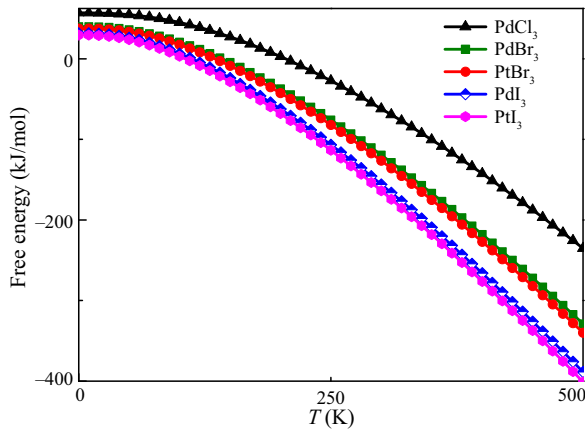

FIG. 2. The calculated temperature-dependent free energy of PdBr$_3$, PtBr$_3$, PdI$_3$, and PtI$_3$ monolayers, where PdCl$_3$ is included for comparison.
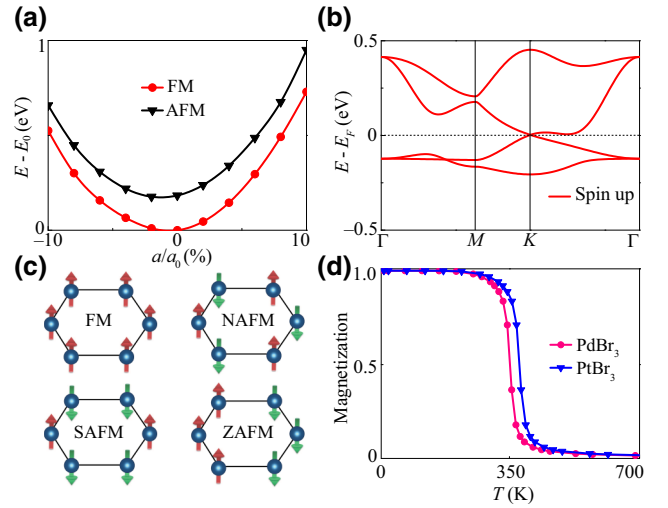

FIG. 3. Half-ferromagnetic PdBr$_3$ and PtBr$_3$ monolayers with Curie temperatures above room temperature. (a) Total energy of the PdBr$_3$ monolayer as a function of the lattice constant for FM and AFM configurations. (b) Band structure of the PdBr$_3$ monolayer without inclusion of SOC, where the bands for spin-down electrons are too far from the Fermi level to be included. (c) Possible configurations of Pd (Pt) spins on the honeycomb lattice: FM, NAFM, SAFM, and ZAFM. (d) Temperature dependence of the normalized magnetic moment of PdBr$_3$ and PtBr$_3$ monolayers by Monte Carlo simulations.

including paramagnetic (PM), FM, Néel AFM (NAFM), stripe AFM (SAFM), and zigzag AFM (ZAFM) configurations, as shown in Fig. 3(c). The results are summarized in Table II. One can observe that the out-of-plane FM (FM^z) state has the lowest energy among them. We further calculate the energies for FM configurations by rotating the magnetic direction deviated from the z axis, and find that the FM^z state is the most energetically favorable, and shows an Ising behavior of the PdBr$_3$ monolayer.

Thus, the effective Hamiltonian can be described by $H_{\rm spin} = -\sum_{\langle i,j \rangle} J S_i^z S_j^z$, where J represents the nearest-neighbor exchange integral, S_i^z and S_j^z are the spin operators, and $\langle i,j \rangle$ denotes the summation over nearest neighbors. J can be determined by the difference in energies between the ZAFM^z and FM^z configurations

TABLE II. The total energy $E_{\rm tot}$ per unit cell for PdBr$_3$, PtBr$_3$, PdI$_3$, and PtI$_3$ monolayers [in millielectronvolts, relative to $E_{\rm tot}$ of the FM^z (FM^x) ground state] for several spin configurations of Pd (Pt) atoms calculated by the GGA plus SOC plus U method.

	FM^z	NAFM^z	SAFM^z	ZAFM^z	FM^x	FM^y	PM
PdBr$_3$	0.0	141.0	119.8	79.2	8.0	7.7	472.1
PtBr$_3$	0.0	207.5	163.2	84.9	1.8	1.7	313.5

	FM^x	NAFM^x	SAFM^x	ZAFM^x	FM^y	FM^z	PM
PdI$_3$	0.0	110.1	93.7	47.9	0.0	13.8	1306
PtI$_3$	0.0	96.8	67.2	52.4	0.0	5.4	260.7

because the ZAFM^z configuration possesses the lowest energy among those AFM configurations (see Table II), which is estimated to be 79.2 meV for the PdBr$_3$ monolayer and 84.9 meV for the PtBr$_3$ monolayer.

Monte Carlo simulations [44] based on the Ising model are performed to calculate the Curie temperature. The Monte Carlo simulations are performed on a 60×60 2D honeycomb lattice with 10^6 steps for each temperature. The magnetic moment as a function of temperature is shown in Fig. 3(d). It can be seen that the magnetic moment decreases rapidly and vanishes at about 350 K for the PdBr$_3$ monolayer and at about 375 K for the PtBr$_3$ monolayer, indicating that PdBr$_3$ and PtBr$_3$ monolayers can be potential candidates for ferromagnetic semiconductors at room temperature.

In transition-metal compounds, the d orbitals are usually not fully filled and the Coulomb correlation U cannot be ignored. Although accurate values of U for PdBr$_3$ and PtBr$_3$ are not known, the correlation interaction U for $4d$ electrons of Pd atoms in the PdBr$_3$ monolayer should be smaller than the 3 eV of the impurity Pd [45]. The correlation interaction U for $5d$ electrons is typically weak, and a reasonable value is usually less than 1 eV. Thus, we take $U = 2.5$ eV for PdBr$_3$ and $U = 0.5$ eV for PtBr$_3$ in the calculations. The electronic band structures of PdBr$_3$ and PtBr$_3$ monolayers based on GGA plus SOC plus U calculations are plotted in Figs. 4(a) and 4(b), respectively. The SOC opens band gaps E_g of 58.7 and 28.1 meV for the PdBr$_3$ and PtBr$_3$ monolayers, respectively, and E_g/k_B values are higher than room temperature. Because the GGA usually underestimates the band gaps, the HSE06 hybrid functional is also used to check the band gaps. Our calculations show that the band gaps are 100.8 and 45 meV with HSE06 for the PdBr$_3$ and PtBr$_3$ monolayers, respectively.

To investigate the topological properties of PdBr$_3$ and PtBr$_3$ monolayers, we first calculate the gauge-invariant Berry curvature $\Omega_z(K)$ in momentum space. A topologically nontrivial band structure is characterized by a nonzero Chern number C that counts the number of edge states. The Chern number C obtained by integrating the Berry curvature $\Omega_z(K)$ over the Brillouin zone is 1. As expected from a nonzero Chern number, the anomalous Hall conductivity shows a quantized charge Hall plateau of $\sigma_{xy} = Ce^2/h = e^2/h$ as shown in Figs. 4(c) and 4(d).

The Fermi surface of 2D materials can be adjusted by using a gate voltage. It is intriguing to find when the occupancy of electrons decreases by 1, the Chern number becomes -2, while when the occupancy increases by 1, the Chern number is still 1. When the e_g bands are half occupied ($E - E_F \approx 0.35$ eV) or unoccupied ($E - E_F \approx -0.25$ eV), the Chern numbers become 0. Thus, the anomalous Hall conductivity can be tuned by a slight shift of the Fermi level for PdBr$_3$ and PtBr$_3$ monolayers, as shown in Figs. 4(c) and 4(d).
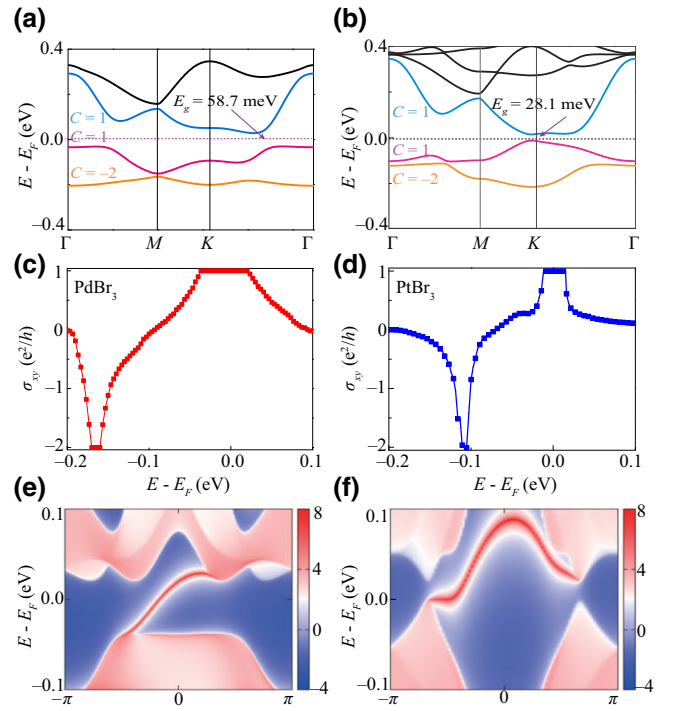

FIG. 4. Room-temperature QAHE in PdBr$_3$ and PtBr$_3$ monolayers. The band structure of (a) PdBr$_3$ and (b) PtBr$_3$ monolayers with SOC, where the Chern number C of nontrivial bands near the Fermi level is indicated, where the band gaps are 58.7 and 28.1 meV for the PdBr$_3$ and PtBr$_3$ monolayers, respectively. Anomalous Hall conductivity of (c) PdBr$_3$ and (d) PtBr$_3$ monolayers as a function of energy near the Fermi level. The surface states of (e) PdBr$_3$ and (f) PtBr$_3$ monolayers. Warmer colors represent higher local density of states, and blue regions indicate the bulk band gap. The results are obtained by GGA plus SOC plus U calculations.

According to the bulk-edge correspondence [46], the nonzero Chern number is closely related to the number of nontrival chiral edge states that emerge inside the bulk gap of a semi-infinite system. As presented in Figs. 4(e) and 4(f), there is one gapless chiral edge state connecting the valence and conduction bands.

To verify the stability of the QAHE against the in-plane strain effect, we also calculate the band structure and Hall conductance of PdBr$_3$ and PtBr$_3$ monolayers for different lattice constants from 5% tensile strain to 5% compression, and find that in these cases the band gap is changed only slightly but not closed, indicating that the QAHE in PdBr$_3$ and PtBr$_3$ monolayers is robust against the strain effect.

III. DISCUSSION

To investigate how robust is the Ising behavior of PdBr$_3$ and PtBr$_3$ monolayers, with the same method, we calculate the magnetic anisotropy of PtBr$_3$, PdBr$_3$, and CrI$_3$ monolayers, where the latter was realized in recent experiments. The energy difference between the in-plane and

out-of-plane ferromagnetic configurations is about 3.6 eV per unit cell for the CrI$_3$ monolayer [47–49], 1.7 eV per unit cell for the PtBr$_3$ monolayer, and 7.7 eV per unit cell for the PdBr$_3$ monolayer. The CrI$_3$ monolayer has been verified to have Ising-type ferromagnetism with out-of-plane magnetization. The PdBr$_3$ monolayer should have Ising-type ferromagnetism with stronger anisotropy than CrI$_3$. To study the PtBr$_3$ monolayer, we take the Hamiltonian given in Ref. [50], where both Kitaev interaction and single-ion anisotropy were considered, by which the Ising behavior of CrI$_3$ [47–49] and the Heisenberg behavior of CrGeTe$_3$ [49,51–53] can be interpreted. Our results show that for the PtBr$_3$ monolayer, both Kitaev anisotropy and single-ion anisotropy are numerically found to be negative, which determines the Ising-type behavior of the PtBr$_3$ monolayer with out-of-plane magnetization.

To check the influence of the Coulomb interaction U on the band gaps, we calculate the bands using the GGA plus SOC plus U method with different values of U for PdBr$_3$ and PtBr$_3$ monolayers. The results show that the band gap changes from 61.3 to 56.9 meV with U ranging from 2 to 3 eV for the PdBr$_3$ monolayer and from 28.1 to 33.7 meV with U ranging from 0.5 to 1 eV for the PtBr$_3$ monolayer. In all cases, the semiconducting state is maintained. Note that typical values of U for 4d and 5d transition metals are used here. The GGA-type calculation usually underestimates the band gap, and the hybrid-functional (such as HSE06) calculation can give values approaching the experimental result. By the HSE06 method, we find that the band gaps are 100.8 and 45 meV for the PdBr$_3$ and PtBr$_3$ monolayers, respectively. As a result, the semiconducting states for PdBr$_3$ and PtBr$_3$ monolayers are robust.

The band gap is opened due to the SOC. The SOC in the Pd(4d) atom is much smaller than that in the Pt(5d) atom. However, one may see a larger band gap for PdBr$_3$ [Fig. 4(a)] and a smaller band gap for PtBr$_3$ [Fig. 4(b)]. To understand this puzzle, we study the dependence of the band gap on on-site Coulomb interaction U for PdBr$_3$ and PtBr$_3$ monolayers by the GGA plus SOC plus U calculations. The band gap, which originates from SOC, increases with the on-site Coulomb interaction U. Consider the Coulomb interaction between the orbitals with the same spin σ, which is given by $H_{F\sigma} = (U' - J_H)[\bar{n}^2 - \frac{1}{4}\lambda_{\mathrm{SOC}}^2(\bar{F})^2\sigma^2(\delta n)^2]$, where U (U') is the on-site Coulomb repulsion within (between) the orbitals and J_H is the Hund coupling between the orbitals. The relationship $U = U' + 2J_H$ [54] holds in the atomic limit. To compensate the interaction, the band splitting due to SOC will increase with increasing U. The enhancement (renormalization effect) of SOC due to Coulomb interaction U was also discussed in the spin Hall effect in Au metal with Fe impurity [55]. The increased U will produce the enhanced SOC, which will induce the increased band gap. The larger band gap and larger anisotropy in the 4d compound PdBr$_3$ come mainly from the larger renormalization effect of SOC

of the Pd atom with a larger U value in PdBr$_3$. The calculation of the U dependence of the Curie temperature shows that when the Coulomb interaction of the PdBr$_3$ monolayer ranges from 1 to 3 eV, the Curie temperature changes from 310 to 383 K, and when the Coulomb interaction of the PtBr$_3$ monolayer ranges from 0 to 1 eV, the Curie temperature changes from 340 to 400 K, which is much higher than room temperature, while in both cases the QAHE is preserved.

Calculations for PdI$_3$ and PtI$_3$ monolayers are performed by the same method as for the PtBr$_3$ and PdBr$_3$ monolayers. There are no imaginary frequencies for the PdI$_3$ and PtI$_3$ monolayers, indicating that they are also dynamically stable. The stability of these two monolayers is also checked by the formation energy (Table I) and free energy (Fig. 2). The PdI$_3$ and PtI$_3$ monolayers both show in-plane magnetization, and the Curie temperatures are estimated [56] to be 150 and 164 K, respectively, which are higher than the Curie temperatures in the present experiments.

Based on 2D room-temperature magnetic semiconductors with a QAHE, new spintronic devices can be designed. For example, by magnetic and spin-orbit proximity effects in bilayer junctions, we can design new functional spintronic devices and overcome various limitations [57].

IV. CONCLUSIONS

On the basis of first-principles calculations, we report that PdBr$_3$ and PtBr$_3$ monolayers are room-temperature out-of-plane ferromagnetic semiconductors with Curie temperatures of 350 and 375 K, respectively. The room-temperature QAHE can also be realized in 2D PdBr$_3$ and PtBr$_3$, with energy band gaps of 58.7 and 28.1 meV, respectively, determined by the GGA and 100.8 and 45 meV, respectively, determined by the HSE06 method. The large band gaps come from multiorbital electron correlations. Bulk PtBr$_3$ was first synthesized a long time ago. By some effort, the experimental realization of 2D PtBr$_3$ crystals may also be possible. Therefore, we expect that the 2D room-temperature ferromagnetic semiconductors PdBr$_3$ and PtBr$_3$ with a QAHE predicted in the present work can be used in experiments soon. By use of room-temperature ferromagnetic semiconductors with a QAHE, progress in developing spintronic devices and dissipationless devices is highly expected.

---

[1] D. Kennedy, What don't we know? Science **309,** 75 (2005).

[2] T. Dietl and H. Ohno, Dilute ferromagnetic semiconductors: Physics and spintronic structures, Rev. Mod. Phys. **86,** 187 (2014).

[3] K. S. Burch, D. Mandrus, and J.-G. Park, Magnetism in two-dimensional van der waals materials, Nature **563,** 47 (2018).

[4] F. D. M. Haldane, Model for a Quantum Hall Effect Without Landau Levels: Condensed-matter Realization of the "Parity Anomaly", Phys. Rev. Lett. **61,** 2015 (1988).

[5] M. Onoda and N. Nagaosa, Quantized Anomalous Hall Effect in Two-dimensional Ferromagnets: Quantum Hall Effect in Metals, Phys. Rev. Lett. **90,** 206601 (2003).

[6] C.-X. Liu, X.-L. Qi, X. Dai, Z. Fang, and S.-C. Zhang, Quantum Anomalous Hall Effect in Hg1-yMnyTe Quantum Wells, Phys. Rev. Lett. **101,** 146802 (2008).

[7] K. He, Y. Wang, and Q.-K. Xue, Topological materials: Quantum anomalous hall system, Annu. Rev. Condens. Matter Phys. **9,** 329 (2018).

[8] C.-X. Liu, S. C. Zhang, and X. L. Qi, The quantum anomalous hall effect: Theory and experiment, Annu. Rev. Condens. Matter Phys. **7,** 301 (2016).

[9] X. Kou, Y. Fan, M. Lang, P. Upadhyaya, and K. L. Wang, Magnetic topological insulators and quantum anomalous hall effect, Solid State Commun. **215-216,** 34 (2015).

[10] J. Wu, J. Liu, and X.-J. Liu, Topological Spin Texture in a Quantum Anomalous Hall Insulator, Phys. Rev. Lett. **113,** 136403 (2014).

[11] C. Wu, Orbital Analogue of the Quantum Anomalous Hall Effect Inp-band Systems, Phys. Rev. Lett. **101,** 186807 (2008).

[12] R. Yu, W. Zhang, H.-J. Zhang, S.-C. Zhang, X. Dai, and Z. Fang, Quantized anomalous hall effect in magnetic topological insulators, Science **329,** 61 (2010).

[13] C.-Z. Chang *et al.*, Experimental observation of the quantum anomalous hall effect in a magnetic topological insulator, Science **340,** 167 (2013).

[14] C.-Z. Chang, J. Zhang, M. Liu, Z. Zhang, X. Feng, K. Li, L.-L. Wang, X. Chen, X. Dai, Z. Fang, X.-L. Qi, S.-C. Zhang, Y. Wang, K. He, X.-C. Ma, and Q.-K. Xue, Thin films of magnetically doped topological insulator with carrier-independent long-range ferromagnetic order, Adv. Mater. **25,** 1065 (2013).

[15] L. Si, O. Janson, G. Li, Z. Zhong, Z. Liao, G. Koster, and K. Held, Quantum Anomalous Hall State in Ferromagnetic SrRuO3 (111) Bilayers, Phys. Rev. Lett. **119,** 026402 (2017).

[16] C. L. Kane and E. J. Mele, Quantum Spin Hall Effect in Graphene, Phys. Rev. Lett. **95,** 226801 (2005).

[17] C. Weeks, J. Hu, J. Alicea, M. Franz, and R. Wu, Engineering a Robust Quantum Spin Hall State in Graphene via Adatom Deposition, Phys. Rev. X **1,** 021001 (2011).

[18] M. Gmitra, D. Kochan, P. Hogl, and J. Fabian, Trivial and inverted dirac bands and the emergence of quantum spin hall states in graphene on transition-metal dichalcogenides, Phys. Rev. B **93,** 155104 (2016).

[19] J. Zhang, B. Zhao, Y. Yao, and Z. Yang, Robust quantum anomalous hall effect in graphene-based van der waals heterostructures, Phys. Rev. B **92,** 165418 (2015).

[20] Z. Qiao, W. Ren, H. Chen, L. Bellaiche, Z. Zhang, A. H. MacDonald, and Q. Niu, Quantum Anomalous Hall Effect in Graphene Proximity Coupled to an Antiferromagnetic Insulator, Phys. Rev. Lett. **112,** 116404 (2014).

[21] H. Zhang, C. Lazo, S. Blugel, S. Heinze, and Y. Mokrousov, Electrically Tunable Quantum Anomalous Hall Effect in Graphene Decorated by 5d transition-metal Adatoms, Phys. Rev. Lett. **108,** 056802 (2012).

[22] X.-L. Zhang, L.-F. Liu, and W.-M. Liu, Quantum anomalous hall effect and tunable topological states in 3d transition metals doped silicene, Sci. Rep. **3,** 2908 (2013).

[23] S.-C. Wu, G. Shan, and B. Yan, Prediction of Near-room-temperature Quantum Anomalous Hall Effect on Honeycomb Materials, Phys. Rev. Lett. **113,** 256401 (2014).

[24] C.-Z. Chang, W. Zhao, D. Y. Kim, H. Zhang, B. A. Assaf, D. Heiman, S.-C. Zhang, C. Liu, M. H. W. Chan, and J. S. Moodera, High-precision realization of robust quantum anomalous hall state in a hard ferromagnetic topological insulator, Nat. Mater. **14,** 473 (2015).

[25] Y. Ou, C. Liu, G. Jiang, Y. Feng, D. Zhao, W. Wu, X.-X. Wang, W. Li, C. Song, L.-L. Wang, W. Wang, W. Wu, Y. Wang, K. He, X.-C. Ma, and Q.-K. Xue, Enhancing the quantum anomalous hall effect by magnetic codoping in a topological insulator, Adv. Mater. **30,** 1703062 (2017).

[26] M. Mogi, R. Yoshimi, A. Tsukazaki, K. Yasuda, Y. Kozuka, K. S. Takahashi, M. Kawasaki, and Y. Tokura, Magnetic modulation doping in topological insulators toward higher-temperature quantum anomalous hall effect, Appl. Phys. Lett. **107,** 182401 (2015).

[27] X. Liu, H.-C. Hsu, and C.-X. Liu, In-plane Magnetization-induced Quantum Anomalous Hall Effect, Phys. Rev. Lett. **111,** 086802 (2013).

[28] Z. Liu, G. Zhao, B. Liu, Z. F. Wang, J. Yang, and F. Liu, Intrinsic Quantum Anomalous Hall Effect with In-plane Magnetization: Searching Rule and Material Prediction, Phys. Rev. Lett. **121,** 246401 (2018).

[29] J. He, S. Ma, P. Lyu, and P. Nachtigall, Unusual dirac half-metallicity with intrinsic ferromagnetism in vanadium trihalide monolayers, J. Mater. Chem. C **4,** 2518 (2016).

[30] C. Huang, J. Zhou, H. Wu, K. Deng, P. Jena, and E. Kan, Quantum anomalous hall effect in ferromagnetic transition metal halides, Phys. Rev. B **95,** 045113 (2017).

[31] J. He, X. Li, P. Lyu, and P. Nachtigall, Near-room-temperature chern insulator and dirac spin-gapless semiconductor: Nickel chloride monolayer, Nanoscale **9,** 2246 (2017).

[32] Q. Sun and N. Kioussis, Prediction of manganese trihalides as two-dimensional dirac half-metals, Phys. Rev. B **97,** 094408 (2018).

[33] Y.-P. Wang, S.-S. Li, C.-W. Zhang, S.-F. Zhang, W.-X. Ji, P. Li, and P.-J. Wang, High-temperature dirac half-metal

PdCl3: a promising candidate for realizing quantum anomalous hall effect, J. Mater. Chem. C **6**, 10284 (2018).

[34] L. Wöhler and F. Müller, Die binären Bromide und Jodide des Platins, Z. Anorg. Allg. Chem. **149**, 377 (1925).

[35] G. Thiele and P. Woditsch, Platin(III)-bromid – ein neuer strukturtyp von AB3-verbindungen, Angew. Chem. **81**, 706 (1969).

[36] G. Kresse and J. Hafner, Ab initiomolecular dynamics for open-shell transition metals, Phys. Rev. B **48**, 13115 (1993).

[37] G. Kresse and J. Furthmuller, Efficient iterative schemes forab initiototal-energy calculations using a plane-wave basis set, Phys. Rev. B **54**, 11169 (1996).

[38] J. P. Perdew, K. Burke, and M. Ernzerhof, Generalized Gradient Approximation Made Simple, Phys. Rev. Lett. **77**, 3865 (1996).

[39] A. Togo and I. Tanaka, First principles phonon calculations in materials science, Scr. Mater. **108**, 1 (2015).

[40] A. A. Mostofi, J. R. Yates, G. Pizzi, Y.-S. Lee, I. Souza, D. Vanderbilt, and N. Marzari, An updated version of wannier90: A tool for obtaining maximally-localised wannier functions, Comput. Phys. Commun. **185**, 2309 (2014).

[41] X. Kong, L. Li, O. Leenaerts, X.-J. Liu, and F. M. Peeters, New group-v elemental bilayers: A tunable structure model with four-, six-, and eight-atom rings, Phys. Rev. B **96**, 035123 (2017).

[42] M. P. L. Sancho, J. M. L. Sancho, J. M. L. Sancho, and J. Rubio, Highly convergent schemes for the calculation of bulk and surface green functions, J. Phys. F: Met. Phys. **15**, 851 (1985).

[43] Q. Wu, S. Zhang, H.-F. Song, M. Troyer, and A. A. Soluyanov, Wannier tools: An open-source software package for novel topological materials, Comput. Phys. Commun. **224**, 405 (2018).

[44] U. Wolff, Collective Monte Carlo Updating for Spin Systems, Phys. Rev. Lett. **62**, 361 (1989).

[45] I. V. Solovyev, P. H. Dederichs, and V. I. Anisimov, Corrected atomic limit in the local-density approximation and the electronic structure ofdimpurities in Rb, Phys. Rev. B **50**, 16861 (1994).

[46] Y. Hatsugai, Chern Number and Edge States in the Integer Quantum Hall Effect, Phys. Rev. Lett. **71**, 3697 (1993).

[47] R. B. Griffiths, Peierls proof of spontaneous magnetization in a two-dimensional ising ferromagnet, Phys. Rev. **136**, A437 (1964).

[48] B. Huang, G. Clark, E. Navarro-Moratalla, D. R. Klein, R. Cheng, K. L. Seyler, D. Zhong, E. Schmidgall, M. A. McGuire, D. H. Cobden, W. Yao, D. Xiao, P. Jarillo-Herrero, and X. Xu, Layer-dependent ferromagnetism in a van der waals crystal down to the monolayer limit, Nature **546**, 270 (2017).

[49] N. Samarth, Magnetism in flatland, Nature **546**, 216 (2017).

[50] C. Xu, J. Feng, H. Xiang, and L. Bellaiche, Interplay between kitaev interaction and single ion anisotropy in ferromagnetic CrI3 and CrGeTe3 monolayers, npj Comput. Mater. **4**, 524 (2018).

[51] N. D. Mermin and H. Wagner, Absence of Ferromagnetism or Antiferromagnetism in one- or Two-dimensional Isotropic Heisenberg Models, Phys. Rev. Lett. **17**, 1133 (1966).

[52] W. Xing, Y. Chen, P. M. Odenthal, X. Zhang, W. Yuan, T. Su, Q. Song, T. Wang, J. Zhong, S. Jia, X. C. Xie, Y. Li, and W. Han, Electric field effect in multilayer cr2ge2te6: A ferromagnetic 2d material, 2D Mater. **4**, 024009 (2017).

[53] C. Gong, L. Li, Z. Li, H. Ji, A. Stern, Y. Xia, T. Cao, W. Bao, C. Wang, Y. Wang, Z. Q. Qiu, R. J. Cava, S. G. Louie, J. Xia, and X. Zhang, Discovery of intrinsic ferromagnetism in two-dimensional van der waals crystals, Nature **546**, 265 (2017).

[54] S. Maekawa, T. Tohyama, S. E. Barnes, S. Ishihara, W. Koshibae, and G. Khaliullin, in *Physics of Transition Metal Oxides*, edited by Maekawa (Springer, Berlin Heidelberg, 2004).

[55] B. Gu, J.-Y. Gan, N. Bulut, T. Ziman, G.-Y. Guo, N. Nagaosa, and S. Maekawa, Quantum Renormalization of the Spin Hall Effect, Phys. Rev. Lett. **105**, 086401 (2010).

[56] D. Spirin and Y. Fridman, 2D ferromagnetic models with symmetry-breaking interactions: Self-consistent harmonic approximation, Physica B **325**, 410 (2003).

[57] I. Žutić, A. Matos-Abiague, B. Scharf, H. Dery, and K. Belashchenko, Proximitized materials, Mater. Today **22**, 85 (2019).